

# Tuning the Work Function of Polar Zinc Oxide Surfaces using Modified Phosphonic Acid Self-Assembled Monolayers

Ilja Lange, Sina Reiter, Michael Pätzel, Anton Zykov, Alexei Nefedov, Jana Hildebrandt, Stefan Hecht, Stefan Kowarik, Christof Wöll, Georg Heimel, and Dieter Neher\*

Zinc oxide (ZnO) is regarded as a promising alternative material for transparent conductive electrodes in optoelectronic devices. However, ZnO suffers from poor chemical stability. ZnO also has a moderate work function (WF), which results in substantial charge injection barriers into common (organic) semiconductors that constitute the active layer in a device. Controlling and tuning the ZnO WF is therefore necessary but challenging. Here, a variety of phosphonic acid based self-assembled monolayers (SAMs) deposited on ZnO surfaces are investigated. It is demonstrated that they allow for tuning the WF over a wide range of more than 1.5 eV, thus enabling the use of ZnO as both the hole-injecting and electron-injecting contact. The modified ZnO surfaces are characterized using a number of complementary techniques, demonstrating that the preparation protocol yields dense, well-defined molecular monolayers.

## 1. Introduction

Over the last years, zinc oxide (ZnO) has attracted significant attention as a transparent, conductive and cheap electrode, and as a potential alternative to indium tin oxide (ITO) in organic optoelectronic devices.<sup>[1–4]</sup> In contrast to ITO, ZnO additionally offers the opportunity to prepare atomically smooth surfaces, thereby enabling the investigation of charge transfer processes at the ZnO/organic semiconductor (OSC) heterojunction with

well-defined interface geometry and energetics. In addition, in recent years a considerable insight into the chemistry and physics of ZnO-surfaces has been gained by detailed surface science studies.<sup>[5]</sup> However, the main drawback is the rather moderate work function (WF) of bare ZnO of roughly 4.3 eV. As a result, when ZnO is brought into contact with a conventional OSC, the Fermi level ( $E_F$ ), which is close to the conduction band in n-type ZnO, will be located within the energy gap between the highest occupied and the lowest unoccupied molecular orbital (HOMO and LUMO, respectively) of the OSC, resulting in significant barriers for hole- or electron injection.<sup>[2,4,6,7]</sup> Hence, schemes to alter the WF of ZnO in a reliable, reproducible

and predictable way are needed. Unfortunately, due to the poor chemical stability of the ZnO-surface, a WF modification with conventional buffer layers, such as poly(3,4-ethylenedioxythiophene):poly(styrenesulfonate) (PEDOT:PSS), has been reported to be not appropriate.<sup>[1,8,9]</sup>

An alternative approach to modify the WF is to shift the electrostatic potential at the surface via attachment of an electric dipole layer. Self-assembled monolayers (SAMs) of various polar molecules have been intensively studied and successfully employed, both experimentally and theoretically, to modify the WF of different metals or metal oxides.<sup>[10–15]</sup> For example, Hotchkiss et al. applied a range of fluorinated benzyl phosphonic acids (BPAs) to tune the WF of ITO over 1.2 eV.<sup>[11]</sup> Whereas a large collection of data exists for SAMs on ITO and other metal oxide surfaces such as  $\text{SiO}_x$  or  $\text{AlO}_x$ , there are comparably only few systematic studies on ZnO in the literature. In order to attach the molecules to the ZnO surfaces, several anchoring groups including carboxylic acids,<sup>[16–18]</sup> amines,<sup>[19]</sup> silanes,<sup>[20,21]</sup> thiols,<sup>[22–26]</sup> or phosphonic acids (PAs)<sup>[15,25–29]</sup> have been utilized. Recent studies proved that particularly thiols and PAs form SAMs at ZnO surfaces.<sup>[25,26]</sup> Experimental and theoretical work has demonstrated a more robust binding of the phosphonic acids compared to thiols, due to the preferential tridentate binding on ZnO.<sup>[25,27–29]</sup>

Recent publications proved the ability of tuning the WF of various ZnO surfaces by such molecular modifications. Bulusu et al. altered the WF of ZnO prepared by plasma atomic layer desposition (ALD) by pentafluorobenzyl

I. Lange, S. Reiter, Prof. D. Neher  
Institute of Physics and Astronomy  
University of Potsdam  
Karl-Liebknecht-Strasse 24–25  
14476, Potsdam, Germany  
E-mail: neher@uni-potsdam.de

Dr. M. Pätzel, J. Hildebrandt, Prof. S. Hecht  
Department of Chemistry & IRIS Adlershof  
Humboldt-Universität zu Berlin  
Brook-Taylor-Str. 2, 12489, Berlin, Germany  
A. Zykov, Prof. S. Kowarik, Dr. G. Heimel  
Institut für Physik  
Humboldt-Universität zu Berlin  
Brook-Taylor-Str. 6, 12489, Berlin, Germany

Dr. A. Nefedov, Prof. C. Wöll  
Institute of Functional Interfaces  
Karlsruhe Institute of Technology  
76344, Eggenstein-Leopoldshafen, Germany



DOI: 10.1002/adfm.201401493

phosphonic acid (5FBPA).<sup>[15]</sup> The mixture of two triethoxysilanes with opposite molecular dipole alignment enabled Brenner et al. to vary the WF of sol-gel processed ZnO by about 0.5 eV.<sup>[30]</sup> Kedem et al. were able to tune the WF of five differently prepared ZnO samples over 1.1 eV by using different phenyl phosphonic acids (PPA).<sup>[31]</sup> A detailed theoretical investigation by density functional theory (DFT) calculations by Wood et al. supports the possibility of systematically shifting the ZnO WF with a variety of fluorine-modified BPAs, thereby also referring to the particular possible binding geometries and orientations.<sup>[29]</sup>

On the other hand, the understanding of the physical properties of SAM-functionalized ZnO is still at an early stage, which is in part caused by the lack of reliable procedures for monolayer formation. For example PAs are believed to form the most robust binding to the ZnO, but particularly these molecules are often reported to cause etching effects at the ZnO surface.<sup>[15,32]</sup> This problem will be discussed later in this article. Furthermore, different preparation techniques are suggested, ranging from dip coating<sup>[22–26,28]</sup> via tethering by aggregation and growth (T-BAG)<sup>[27]</sup> to spray coating<sup>[15]</sup> with no consensus about the most suitable approach.

Moreover, a detailed investigation of the surface coverage and the molecular orientation of the molecules in the SAM, in particular on intrinsic ZnO, is virtually missing. In recent studies, near-edge X-ray absorption fine structure (NEXAFS) spectroscopy and/or infrared absorption reflection spectroscopy (IRRAS) were used to determine the molecular orientation of thiols and phosphonic acids only on aluminium-doped ZnO (AZO) or indium zinc oxide (IZO) surfaces.<sup>[24,33]</sup> However, because the major part of studies on ZnO modifications has been performed on sputtered or sol-gel prepared ZnO with rough ill-defined surfaces, many surface-analyzing techniques are therefore hardly applicable on such pure ZnO.

Here, we report on the formation of SAMs from various modified PAs on well-defined ZnO single crystal surfaces. Though single crystals might be irrelevant for commercial applications, their well-defined surface (in contrast to sputtered or sol-gel processed ZnO layers) renders them particularly well suited for the development of reproducible protocols for SAM deposition and for gaining access to fundamental structural properties. Such a protocol is developed for the generic modification of polar ZnO-surfaces, thereby preventing the frequently appearing etching effects at these surfaces. The high quality of the so-prepared SAMs is proven by angle-dependent NEXAFS,

X-ray reflectivity (XRR) measurements, Kelvin Probe (KP), atomic force microscopy (AFM), and scanning Kelvin Probe microscopy (SKPM), pointing towards a dense and homogeneous coverage of the ZnO surface with a monolayer of well-oriented molecules. By employing PAs with functionalities covering a wide range of dipole moments, we are able to alter the ZnO WF by more than 1.5 eV, from 4.1 eV to almost 5.7 eV. This allows us to continuously tune the ZnO charge injection properties, enabling the application of ZnO as both electron and hole injecting contact. We find that changing the ZnO work function alters the unipolar currents in P3HT and PCBM-based diodes by five orders of magnitude, which highlights the very high quality of our SAM-functionalized ZnO surfaces.

## 2. Results and Discussion

### 2.1. Materials and Molecular Dipole Moments

For our experiments, polished and properly annealed Zn-terminated ZnO (0001) or O-terminated (000-1)-ZnO single crystals with the dimensions  $10 \times 10 \times 0.5 \text{ mm}^3$  were used (see the Experimental Section for details). To tune the WF over a wide range, we tested a variety of BPAs with chemical modifications at different positions of the molecule and, therefore, different dipole moments. In addition we employed a new class of phosphonic acids based on pyrimidine, with the goal to further lower the WF of ZnO. Pyrimidine derivatives have already been discussed in literature as a means to alter the substrate WF and, therefore, the charge carrier injection properties.<sup>[34,35]</sup> Here, we apply a non-substituted pyrimidine PA (PyPA) as a representative of this promising class of PA-based molecules. The chemical structures of all used molecules are displayed in **Figure 1**, together with the value of the dipole moment of the head group (the substituted aromatic ring) as calculated using density functional theory (DFT). For the full chemical names of all molecules see the Experimental Section.

According to the work of Li et al., the total change in WF upon SAM attachment,  $\Delta\Phi_{\text{tot}}$ , is determined by the sum of the following contributions

$$\Delta\Phi_{\text{tot}} = \Delta\Phi_{\text{SAM}} + \Delta\Phi_{\text{chem.bond.}} + \Delta\Phi_{\text{geom.rec.}} \quad (1)$$

with  $\Delta\Phi_{\text{SAM}}$  indicating the shift of the electrostatic potential caused by the dipole moment of the molecules in the isolated

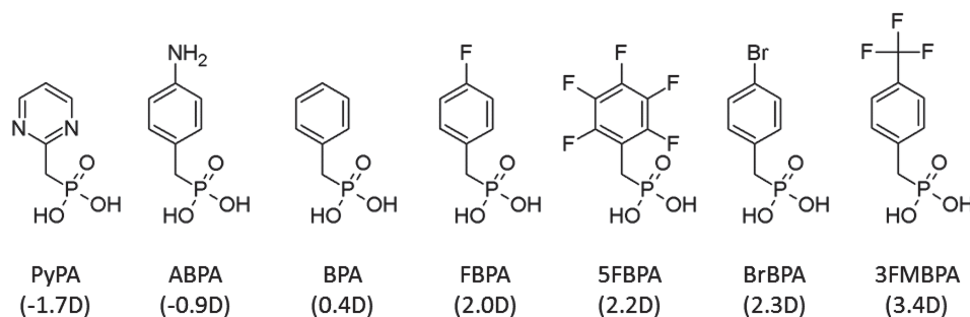


**Figure 1.** Chemical structures and acronyms of all applied phosphonic acids, with their respective dipole moments of the head group  $\mu_{\text{head}}$  shown in the brackets. A negative sign indicates that the negative pole points towards the PA anchoring group.

SAM,  $\Delta\Phi_{\text{chem.bond.}}$  the contribution of the charge redistribution at the interface due to the chemical binding of the molecules to the substrate, and  $\Delta\Phi_{\text{geom.rec.}}$  the WF shift of the substrate with respect to the bare surface due to geometry relaxation upon SAM adsorption.<sup>[36]</sup> The relation between  $\Delta\Phi_{\text{SAM}}$  and the molecular dipole moment  $\mu$  is given by the Helmholtz equation

$$\Delta\Phi_{\text{SAM}} = \frac{e\mu_{\perp}}{\epsilon_0 k_{\text{red}}} \frac{N}{A} \quad (2)$$

where  $e$  denotes the elementary charge,  $\mu_{\perp}$  is the dipole moment component perpendicular to the surface,  $N/A$  denotes the number of dipoles per area, and  $\epsilon_0$  is the vacuum permittivity. Note that a close arrangement of the molecular dipoles causes a strong interaction with their respective electric fields. This interaction suppresses the individual dipole moments of the densely packed molecules compared to the ones in the gas phase.<sup>[37–42]</sup> To account for this depolarization, a reduction factor  $k_{\text{red}}$  has to be included into Equation (2).

The dipole moment vector  $\vec{\mu}$  can be further decomposed into a contribution of the head group,  $\vec{\mu}_{\text{head}}$ , and a contribution of the anchoring group,  $\vec{\mu}_{\text{anchor}}$ . Our DFT calculations suggest that the  $\text{CH}_2$  group between the PA and the benzyl ring largely decouples these two parts electronically and, therefore, the total dipole moment  $\vec{\mu}$  is roughly the sum of  $\vec{\mu}_{\text{head}}$  and  $\vec{\mu}_{\text{anchor}}$ . Theoretical work by Wood et al. also showed that the particular substitution of the benzyl ring has only little effect on the charge distribution within the phosphonic acid anchoring group.<sup>[29]</sup> Their work also revealed comparable tilting angles of  $\vec{\mu}_{\text{head}}$ , independent of the fluorination of BPA. Therefore, for our calculation of  $\vec{\mu}_{\text{head}}$ , the phosphonic acid group was replaced by hydrogen.

As all of the molecules applied here have the same basic structure, no significant variations in the nature of attachment and assembling are expected. Therefore,  $\Delta\Phi_{\text{geom.rec.}}$ ,  $\Delta\Phi_{\text{chem.bond.}}$ , and  $\mu_{\text{anchor}}$  are assumed to be equal and independent of the modification of the head group. The remaining variables are then the absolute value and the tilting angle of  $\vec{\mu}_{\text{head}}$ , as well as the molecular surface coverage, all of which will be addressed in the following sections.

## 2.2. Protocol for SAM Formation

To prepare the SAMs on the ZnO surface, a variety of preparation procedures have been proposed in literature. However, in none of these publications the structural properties of the self-assembled monolayers formed on the ZnO substrates has been thoroughly characterized. Therefore, a major aim of this work was to develop a reliable protocol that leads to well-defined, densely packed monolayers of the molecules without damaging the ZnO surface.

Valtiner et al. showed that pH values <3.8 can lead to etching of the ZnO surface.<sup>[43]</sup> It is, therefore, expected that the ZnO surface is severely disturbed in presence of our phosphonic acids in combination with water. Indeed, we find a strong correlation between the water content, the acidity of the PA-solutions and the quality of the SAM-functionalized ZnO surface. While a 2 mM BPA solution in pure deionized water has a pH  $\approx$  2.5,

use of absolute ethanol (G CHROMASOLV, Sigma Aldrich, 99.9% purity) instead of water decreases the pH to 3.4 and utilization of dried ethanol (SeccoSolv, Merck Millipore, <0.01%  $\text{H}_2\text{O}$ ) further reduces the acidity of the solution to pH  $\approx$  4.3. Immersion in an aqueous BPA solution discolored both the wafer and the solution to milky white, indicating already by the naked eye a very strong etching of the ZnO surface.<sup>[15,32]</sup> Although these effects were strongly reduced when absolute ethanol-BPA solution was applied, more detailed investigations by AFM still revealed a grainy structure with numerous protrusions, pointing to etching effects also in this solution (Figure S2 in the Supporting Information). These protrusions are loosely bound to the ZnO substrate and can easily be laterally displaced by the AFM tip in contact mode, similar to the observations reported earlier by Chen et al.<sup>[26]</sup> Contrarily and most importantly, no such grains were observed when dried ethanol was used (Figure 3). Therefore, such high-purity ethanol was used for the preparation of the SAMs reported in this study.

## 2.3. Work Function Tuning

Following this protocol, the properly prepared ZnO substrates were immersed into solutions of the different phosphonic acids (see Figure 1) in dried ethanol. After immersion, the samples were gently purged in dried ethanol to remove residual (physisorbed) molecules and subsequently dried in a  $\text{N}_2$ -stream followed by an annealing step on a hot plate at 90 °C for 3 min to remove residual ethanol. Work functions were measured with a Kelvin probe (KP) setup calibrated against highly ordered pyrolytic graphite (HOPG), for which we assume a WF of 4.6 eV.<sup>[44]</sup> All KP measurements were performed in a  $\text{N}_2$ -filled glovebox at room temperature, which are also the conditions for OSC deposition. We estimated the conductivity of the undoped ZnO substrates to 3–5  $\text{Sm}^{-1}$ , which is sufficiently large to provide the current during the KP measurements. For BPA, FBPA, 5FBPA, ABPA, and PyPA, the largest shifts in WF was realized after immersing the wafer in dried ethanol for two hours, while keeping the solution at 70 °C for one hour and letting it cool down to room temperature during the second hour. Longer immersion times generally lead to smaller work function shifts, which we attribute to the formation of multilayers. For BrBPA and 3FMBPA, this effect was seen already after 20 min, (Figure S1 in the Supporting Information). Therefore, the immersion time in these two solutions was reduced to 20 min at 70 °C.

Absolute (macroscopic) WFs of optimized SAM-covered ZnO (0001)-Zn and (000-1)-O substrates are related to the head-group dipole moment  $\mu_{\text{head}}$  in Figure 2, the absolute values are displayed in Table 1. The graph shows that the WF is a linear function of  $\mu_{\text{head}}$ . This is fully consistent with the prediction of the Helmholtz-equation (Equation (2)), indicating that the molecular tilt angle and the surface coverage is either constant or it changes only gradually with the dipole moment. By employing molecules with a wide range in dipole moment, we succeeded to alter the ZnO WF by more than 1.5 eV, which is by far the largest reported on ZnO surfaces. Interestingly, very similar WF shifts are seen on substrates with either Zn- or O-terminated surfaces.

It should be noted that a direct comparison with the WF of untreated ZnO is not meaningful. ZnO is known to adsorb

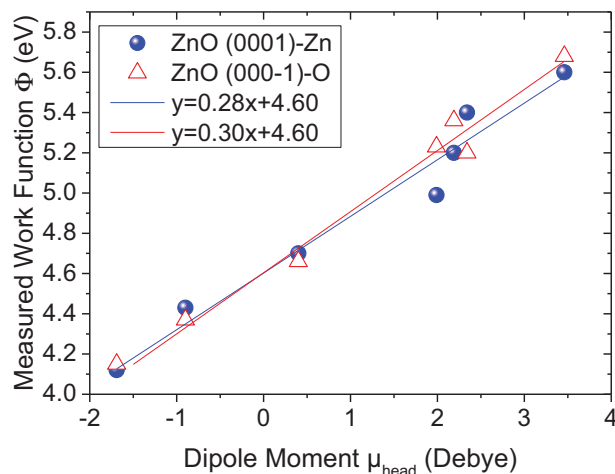


**Figure 2.** WF of ZnO (0001)-Zn and (000-1)-O substrates covered with SAMs from the molecules in Figure 1, plotted as a function of the head group dipole moment  $\mu_{\text{head}}$  (see brackets in Figure 1). All WF values were measured with the Kelvin Probe (KP) technique. Lines are fits to Equation (2). The WF spans a range of about 1.5 eV.

residual contaminations such as  $\text{H}_2$ ,  $\text{H}_2\text{O}$ , or  $\text{CO}_2$  even under ultra-high vacuum conditions,<sup>[5]</sup> which alters the surface. Additionally, it has been shown that even brief exposure of high-purity ZnO substrates to water already leads to H-atom concentrations  $>0.1\%$  in the bulk close to the surface.<sup>[45]</sup> These H-atoms lead to an effective n-doping of this material, which will also affect the WF. As the preparation of our ZnO substrates involves several steps (in different environments and temperatures), it is rather unlikely that the chemistry of the final (non-modified) surface is always the same. Indeed we find a poor reproducibility of the WF of the “clean” ZnO surface and a strong dependence on pre-treatment or storing conditions prior to the measurement. Therefore, a reasonable reference value for bare ZnO is experimentally inaccessible. However, after chemisorption of the SAM the WF became much more reproducible. Notably, ZnO wafers with a well-expressed terraced topography had absolute WFs reproducible within an error of less than  $\pm 50$  meV.

The strict relation between WF and  $\mu_{\text{head}}$  suggests the coverage of the ZnO surface to be reproducible on the macroscopic scale. To evaluate a possible spatial variation in the WF of the SAM-functionalized surfaces, all samples were analyzed by scanning Kelvin probe microscopy (SKPM). In this technique, the probe is formed by the oscillating tip of an atomic force microscope (AFM), enabling a resolution of a few tens of nm. The results are shown in Figure 3 together with the corresponding AFM height profiles.

The AFM height profiles show the terraced structure of the underlying ZnO substrate. As described above, no grainy structure is visible, proving the absence of any etching effects. Also,

no evidence for island- or multiple molecular layer formation is seen in the AFM height profiles. Although multilayer formation by these short molecules might be difficult to be resolved by AFM, any inhomogeneity should strongly affect the local WF shift, and therefore the SKPM signal. In almost all cases, however, the SKPM histogram shows a weak fluctuation of the surface potential within the  $3 \times 3 \mu\text{m}$  scan area of less than  $\pm 40$  meV. The scan of larger areas did not reveal substantially larger variations. The single exception is 5FBPA with a deviation of about  $\pm 60$  meV which might be caused by the presumably lower stability of that molecule under ambient conditions compared to all other molecules applied here. However, as this molecule initiates one of the highest WFs in the achieved range, the deviation relative to the total WF shift is still reasonably low.

We find the overall spread of local Kelvin potential in the SKPM images to be around (or less than) 10% of the respective macroscopic WF shift. Such a weak variation could be caused by, e.g., a variation of the tilting angle of the molecules by up to  $\pm 5^\circ$ . Part of that variation may also stem from inhomogeneities of the underlying substrate, for which we have found fluctuations of the surface potential around the mean value of about  $\pm 15$  meV. To conclude this part of the work, the linear dependence of the WF on the molecular dipole moment and the small variation in the local WF in the SKPM experiments point to a rather homogenous arrangement of the dipoles on the ZnO surface in all cases, at least on the few 10 nm scale.

#### 2.4. Molecular Orientation

In order to characterize the composition of the self-assembled monolayers (SAMs) formed on the ZnO-substrates and to determine the orientation of the monomers within the SAMs relative to the substrate surfaces, near edge X-ray absorption fine structure (NEXAFS) spectra have been recorded for different photon incident angles  $\theta$  with values between  $20^\circ$  and  $90^\circ$ . Figure 4a shows the corresponding C K-edge NEXAFS spectra of BPA on ZnO. We can clearly identify the characteristic benzene  $\pi^*$ -resonance and further features (an assignment is provided in Figure 4a), which serve as a fingerprint of the SAM-forming BPA monomer.<sup>[46]</sup> The transition dipole moment (TDM) governing the excitation of C1s-electrons into the aromatic  $\pi^*$  level is orientated perpendicular to the molecular plane of the aromatic ring. Since the intensity of a NEXAFS-resonance for excitations in such cases is given by the angle between the TDM and the electric field vector of the incident light beam, the orientation of the molecular plane relative to the surface plane can be determined from the variation of the  $\pi^*$  NEXAFS resonance intensity with photon angle of incidence.

In the present case, due to the three-fold symmetry of the substrate the azimuthal orientation can be averaged and the  $\pi^*$  peak area  $I(\theta)$  can be quantitatively analyzed in order to extract

**Table 1.** Absolute WFs of the SAM-modified ZnO substrates.

	PyPA	ABPA	BPA	FBPA	5FBPA	BrBPA	3FMBPA
(0001)-Zn	4.12 eV	4.43 eV	4.70 eV	4.99 eV	5.20 eV	5.40 eV	5.60 eV
(000-1)-O	4.15 eV	4.37 eV	4.66 eV	5.23 eV	5.36 eV	5.21 eV	5.68 eV

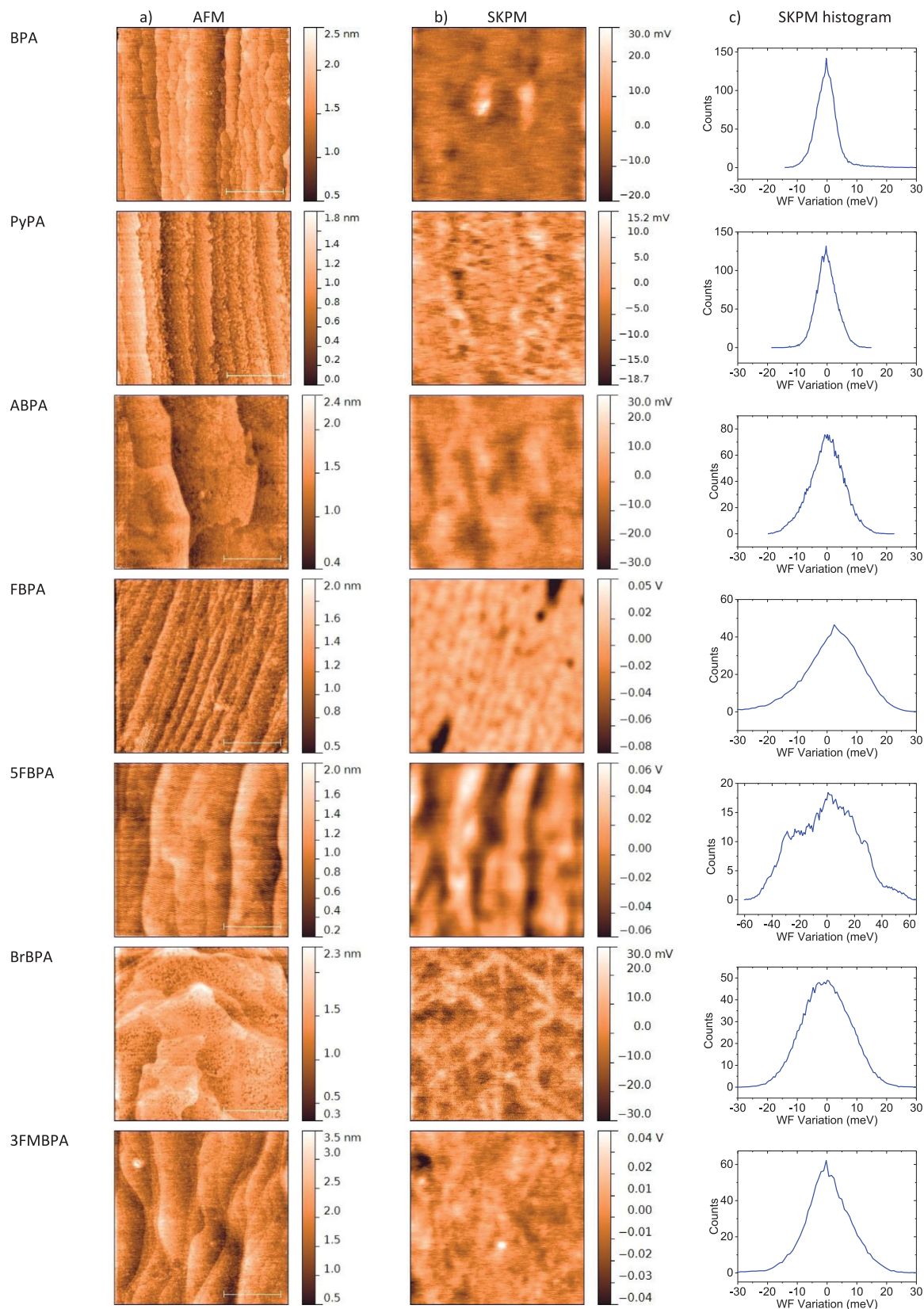


**Figure 3.** a) AFM height profile shows the underlying terraced ZnO structure. The presence of well pronounced terraced surface and the lack of grains at the surface indicates the absence of etching effects. The scanned area is  $3 \times 3 \mu\text{m}^2$  in all cases. b) SKPM images and c) SKPM histogram of the same area showing the variation of the Kelvin potential over the measured area.

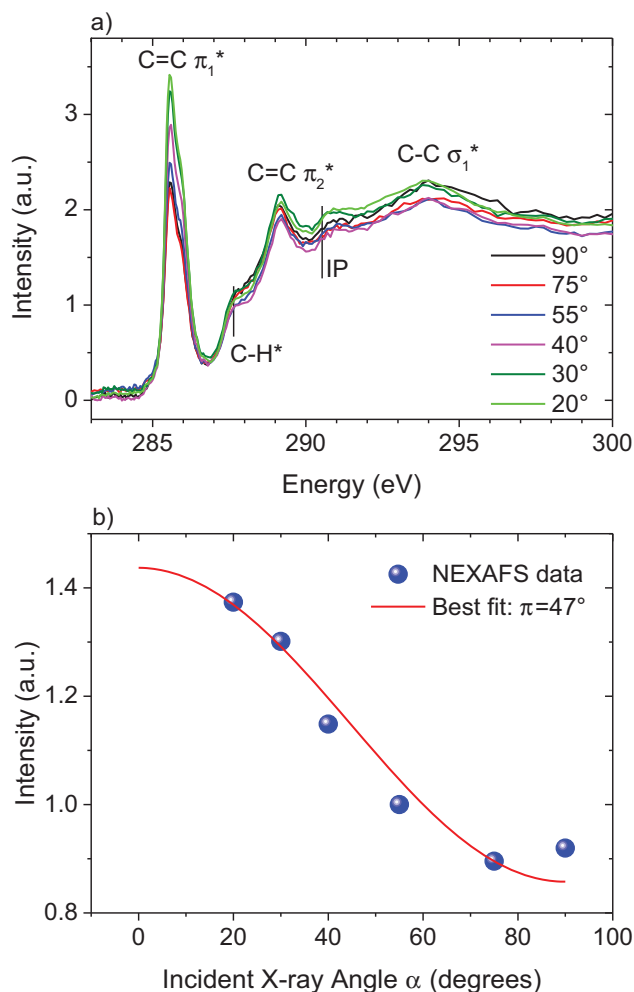


**Figure 4.** a) NEXAFS spectra recorded at different X-ray photon angles of incidence (20°–90°) for BPA SAMs on ZnO (0001)-substrates. b) The angle dependence of  $\pi_1^*$ -transition intensities. The best fit yields  $\alpha = 47^\circ \pm 3^\circ$ .

the tilt angle  $\alpha$  of the aromatic ring with respect to the surface according to

$$I(\theta) \propto P \cos^2(\theta) \left( 1 - \frac{3}{2} \sin^2(\alpha) \right) + \frac{1}{2} \sin^2(\alpha), \quad (3)$$

where  $P$  is the degree of polarization of the incident X-ray light. The angle dependence of the  $\pi_1^*$ -transition intensities is shown in Figure 4b along with the best fit according to Equation (3). The latter is presented by the red curve yielding a tilting angle  $\alpha$  of  $47^\circ \pm 3^\circ$ . Therefore, we can conclude that the molecules are indeed attached to the ZnO surface with a preferential orientation. The value of  $47^\circ \pm 3^\circ$  is in excellent agreement to theoretical DFT calculations by Wood et al. of BPA on ZnO, yielding an angle of the aromatic ring relative to the ZnO surface of  $\alpha = 45.5^\circ$  in case of a tridentate binding.<sup>[29]</sup> These authors claimed a lower tilting angle of  $\alpha = 43.4^\circ$  when the molecules are bound in a bidentate fashion, supporting a preferentially tridentate binding also in our case in accordance with other publications.<sup>[25,27,28]</sup> Note that these calculations also suggest an only

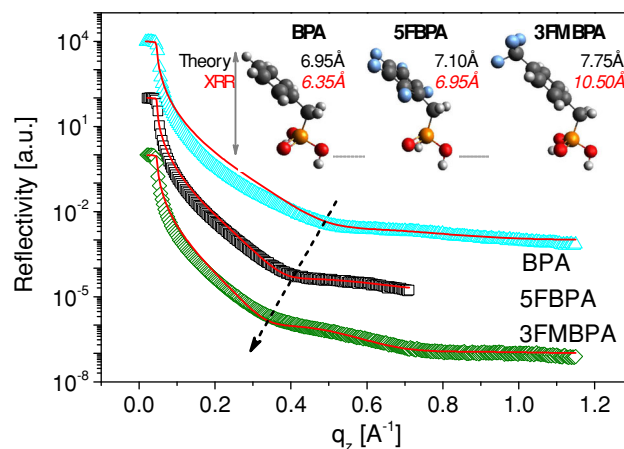


**Figure 5.** XRR measurements of BPA, 5FBPBA and 3FMBPBA on ZnO (0001)-Zn and the correlating fit curves (red lines). The position of the minimum of the Kiessig fringes decreases with increasing SAM thicknesses to smaller values of  $q_z$ , which is indicated by the arrow. The values for the total thicknesses of each SAM based on the theoretical estimate for a tilt of the head group of  $47^\circ$  (as measured by NEXAFS) and deduced from the XRR fits are shown in the inset.

weak effect of the ring substitution on the tilting angle of the aromatic ring relative to the ZnO surface, which was predicted to vary between  $45.1^\circ$  and  $47.4^\circ$  for tridentate binding. Therefore, in the following analysis, we assumed the same experimentally determined molecular tilt of  $47^\circ$  relative to the ZnO surface for all of our PAs.

## 2.5. Thickness of the Layer

To determine the thicknesses of the SAMs and their electron density, X-ray reflectivity (XRR) measurements were performed. In Figure 5 the reflectivity curves of BPA, 5FBPA and 3FMBPA are shown. The edge of total reflection at an out-of-plane scattering vector of about  $q_z = 0.046 \text{ \AA}^{-1}$  closely matches the literature value for ZnO. We furthermore observe the expected decaying Fresnel reflectivity curve and for larger  $q_z$  a slight oscillation in the reflectivity, the so called Kiessig fringes. These fringes originate from thickness interferences between reflections from the top and bottom interfaces of the SAM. The position of the fringe minimum is a measure for the SAM thickness and shifts towards smaller values of  $q_z$  for larger layer thicknesses.

From the Parratt fits to the measured XRR curves the values of SAM thickness and electron density can be quantified. For BPA and 5FBPA the best fits were achieved with a simple one-layer model and by using the tabulated electron densities (NIST database), i.e.,  $\rho_{\text{BPA}} = 0.44 \text{ \AA}^{-3}$  and  $\rho_{\text{5FBPA}} = 0.54 \text{ \AA}^{-3}$ . In the case of 3FMBPA, however, a two-layer model was necessary to achieve a good fit. In a two-layer model one separates the SAM into the head and the anchor group with different electron densities, i.e.,  $\rho_{\text{3FMBPA-head}} = 0.46 \text{ \AA}^{-3}$  and  $\rho_{\text{3FMBPA-tail}} = 0.36 \text{ \AA}^{-3}$ . Such a two layer approach is well known in the literature.<sup>[47]</sup>

The fit curves reproduce the position of the oscillation minimum well for each SAM. The values deduced for the thicknesses of BPA and 5FBPA are  $d_{\text{BPA}} = 6.3 \text{ \AA}$  and  $d_{\text{5FBPA}} = 6.85 \text{ \AA}$ ,

while the sum of the heights of the head and tail group of 3FMBPA results in a total thickness  $d_{3\text{FMBPA}} = 10.5 \text{ \AA}$ . The trend of BPA being the thinnest and 3FMBPA being the thickest layer is in accordance with the theoretical estimations considering a constant tilting angle of the head group of  $47^\circ$  as measured by NEXAFS (see inset of Figure 5). While the measured thicknesses do not perfectly match the theoretically expected SAM heights, the XRR measurements confirm that the investigated molecules form layers on the ZnO surface with an average height of roughly one monolayer, i.e., no multilayers or significant amount of physisorbed molecules are observed.

## 2.6. Surface Density

Having proven the homogeneous coverage of the ZnO surface with a monomolecular SAM, we are now able to provide an estimate of the surface density of molecules using the Helmholtz equation. Unfortunately, as mentioned above, the reference value of bare ZnO is inaccessible and, thus, the absolute WF shift of every individual SAM cannot be quantified directly. Therefore, we made use of the strict linear relation between the WF and the molecular dipole moment by rewriting the Helmholtz Equation (2) in a differential form:

$$\frac{N}{A} = \frac{\epsilon_0 k_{\text{red}}}{e \sin \alpha} \frac{d\Phi}{d\mu} \quad (4)$$

Due to hydroxylation effects<sup>[48]</sup> the reasonable maximum coverage of the ZnO surface with the SAMs is one molecule per unit cell, yielding  $N/A_{\text{max}} = 2.73 \text{ nm}^{-2}$ .<sup>[29]</sup> The lower bound for the surface coverage in our experiments can be estimated by fitting the data of Figure 2 with Equation (4) while setting  $k_{\text{red}}$  to 1 (no depolarization), yielding  $N/A_{\text{min}} = 1 \text{ nm}^{-2}$ . As  $k_{\text{red}}$  is determined by the interaction strength of the neighboring molecules, it is strictly correlated to  $N/A$ . This makes the individual determination of the coverage and  $k_{\text{red}}$  impossible. However, it has been established that a reasonable value for  $k_{\text{red}}$  of such molecular layers is in the range of 1.9–2.<sup>[39]</sup> Therefore, we can conclude that the average surface density in our SAMs is approximately  $2 \text{ nm}^{-2}$ . This value evidences a dense surface coverage, reasonably close to the theoretical maximum, pointing again to a high quality of the SAMs.

It should be noted that the value of  $k_{\text{red}}$  might be affected by the electrostatic interaction between  $\vec{\mu}_{\text{anchor}}$  and the polarizable headgroups of the phosphoric acid molecules. As, however, this effect will be weak in dense molecular layers,<sup>[42]</sup> it can safely be neglected in light of the uncertainty discussed above.

Notably, our surface density is substantially larger than what has been found by Hotchkiss et al. using the same family of BPA-based molecules on ITO.<sup>[11]</sup> By comparison to older results they claim a density of at least  $0.7 \text{ nm}^{-2}$ . However, analyzing their data using Equation (4) reveals a molecular density of about  $1.3 \text{ nm}^{-2}$ . The difference between their and our work is reasonable considering that ITO provides a rough, ill-defined surface, whereas the ZnO substrates used here are single-crystalline and exhibit a smooth surface with low defect density. Our density is also higher than the value recently reported by Li et al. for a ferrocene PA on sputtered Gallium-doped ZnO

(GZO) prepared (ca.  $1.4 \text{ nm}^{-2}$ ).<sup>[49]</sup> This discrepancy is reasonable given that ferrocene is rather bulky and that the surface of the sputtered GZO differs from our single crystalline ZnO wafer surface with regard to topography and surface chemistry.

## 2.7. Single Carrier Devices

As a proof of concept we prepared organic hole- and electron-only devices with the modified ZnO as one injecting electrode and poly(3-hexylthiophene) (P3HT) or phenyl-C71-butyric acid methyl ester (PCBM), respectively, as transporting organic semiconductors. Within the two types of devices, the WF of the ZnO was continuously altered by using different SAMs.

From theory, the current through a unipolar device is either injection or bulk limited. If the electrode Fermi level ( $E_F$ ) is within or approaches the respective transport band of the semiconductor, thermally induced charge transfer takes place, which pins the substrate  $E_F$  at an energy in the OSC band gap close to the band onset<sup>[50–55]</sup> Therefore, irrespective of the particular electrode  $E_F$ , within the pinning regime the contact is Ohmic, resulting in a bulk-limited current with no significant influence of the electrode WF on the current density–voltage ( $J$ – $V$ ) characteristics. In contrast, if the electrode  $E_F$  lies well above the HOMO or well below the LUMO, respectively, a subsequent injection barrier is formed, and the now injection limited current is strongly reduced compared to the above case of an Ohmic contact.

Figure 6 shows the representative  $J$ – $V$  characteristics of single carrier devices with modified ZnO as the bottom electrode. These experiments should be considered as a first proof of principle measurements. Further improvements of the experimental configuration (including a better contact to the ZnO) and the quantitative analysis of the data are subject to future investigations. As the HOMO of P3HT is considered to be at  $4.8 \pm 0.3 \text{ eV}$ ,<sup>[50,56–59]</sup> the high WF ZnO  $\geq 5.2 \text{ eV}$  induced by the application of 3FMBPA, BrBPA or FBPA should lead to Ohmic contacts. Indeed, in Figure 6a these three SAMs give the highest currents among all applied SAMs. The devices with the other SAMs as well as the non-treated ZnO with WFs smaller than  $4.8 \text{ eV}$  show a strong reduction of the currents under forward bias, pointing to injecting-limited currents, which is in accordance with the theory stated above. Consequently, the lowest current is detected for the PyPA modified ZnO electrode with the lowest WF among all SAMs, about five orders of magnitude smaller than for ZnO substrates coated with 3FMBPA, BrBPA or FBPA. Note that in backward direction (hole injection from the positive top silver electrode), no significant variation of the current is observed (within the experimental error).

The exact opposite trend is obtained for the electron-only devices comprising PCBM in Figure 6b. Again, the currents under injection from the modified electrode (the bottom electrode is biased negatively) can be varied over several orders of magnitude, according to a change of the injection barrier. Notably, the lowest injection barriers are now detected if PyPA or ABPA are applied to decrease the ZnO WF, with resulting values of  $4.12 \text{ eV}$  and  $4.4 \text{ eV}$ , respectively. Because the pinning level of pure PCBM prepared under these conditions is at around  $-4.25 \text{ eV}$ ,<sup>[60,61]</sup> it can be expected that also the

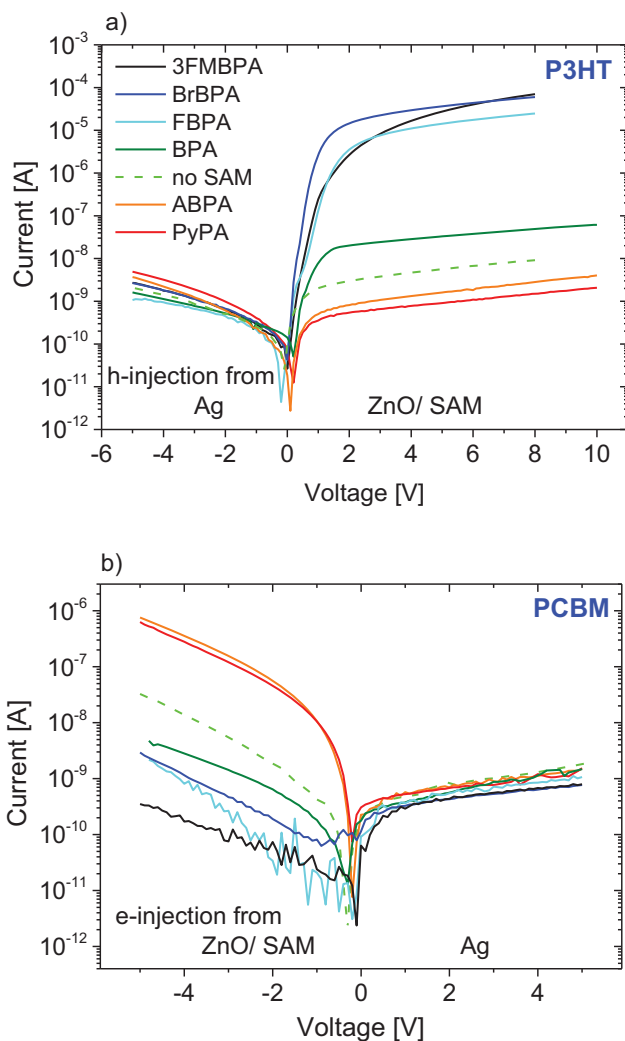


**Figure 6.** *J*–*V* characteristics of single carrier devices in the stack ZnO/SAM/organic semiconductor/Ag with a) P3HT or b) PCBM. The only parameter varied is the WF of the ZnO due to the application of different SAMs. A voltage larger than zero means that a positive bias is applied to the bottom electrode.

ABPA-modified electrode is close or within the pinning regime of the PCBM LUMO. On the other hand, the lowest current is seen for 3FMBPA with the largest resulting WF among all molecules.

### 3. Conclusions

We have successfully used several modified phosphonic acid based molecules to tune the WF of the polar ZnO (0001)-Zn and (000-1)-O surfaces. We have developed a protocol which avoids etching of the ZnO-substrates and which yields well-defined SAMs of reproducible, high quality. The SAMs have been investigated by a manifold of techniques. For the case of BPA-SAMs, NEXAFS results showed that the molecules are attached to the substrate with an average tilt-angle of the phenyl-ring plane relative to the surface of 47°. XRR

measurements revealed thicknesses in good agreement to the formation of molecular monolayers. Results from AFM and SKPM indicated the presence of highly homogeneous films. The analysis of these data revealed a density of the molecules at the ZnO surface of about 2 nm<sup>-2</sup>. Therefore, we can conclude that all phosphonic acid based molecules studied here form a well-ordered, dense SAM at ZnO. A linear shift of the macroscopic WF with the dipole moment of the molecules has been observed spanning a wide range of about 1.5 eV, larger than in previous reports,<sup>[31]</sup> irrespective of whether Zn-terminated ZnO (0001) or O-terminated (000-1)-ZnO is employed. As a proof of concept for the application of ZnO as an injecting electrode in optoelectronic devices, a set of hole-only and electron-only devices was prepared. It is shown for the first time that ZnO can serve as both electron- and hole injecting contact, and that the injection properties can be continuously altered from being strongly injection limited to Ohmic. Importantly, unipolar currents in P3HT and PCBM-based diodes can be tuned by several orders of magnitude by simply controlling the ZnO work function. We presume that this result opens new opportunities for the design of regular and inverted electronic devices and, consequently, for the improvement of such devices. Finally, smooth well-defined ZnO surfaces with widely tunable WF will constitute ideal system for addressing the correlation between surface energetics/chemistry and charge injection capability. By now, most studies on unipolar devices refer to charge injection from the top contact.<sup>[62–66]</sup> In this case, the charge injecting interface is inaccessible to a conclusive characterization of the morphology and energetics. Given the homogeneity and robustness of our functionalized ZnO surfaces, our future studies will be devoted to a detailed understanding of charge injection across the ZnO-organic interface combined with its comprehensive characterization using advanced photoelectron spectroscopy and X-ray absorption techniques.

Added in proof: A recent publication by M. Timpel et al.<sup>[79]</sup> considers the binding of two phosphonic acids, tridecafluorooctyl-PA (F13OPA) and p-(trifluoromethyl)phenyl-PA (pCF-3PhPA) on single crystal ZnO (0001)-Zn surfaces. In contrast to the chemically related compound 3FMBPA studied here, the substituted phenyl ring is directly linked to the PA in pCF-3PhPA, rendering the linkage between the binding site and the aromatic moiety very stiff. As a consequence, Timpel et al. find a preferential bidentate binding of pCF3PhPA at the Zn-terminated ZnO surface and a larger molecular tilt with regard to the substrate plane (when compared to 3FMBPA).

### 4. Experimental and Computational Section

**Substrates:** Zn-terminated ZnO (0001) or O-terminated (000-1)-ZnO single crystals with the dimensions 10 × 10 × 0.5 mm<sup>3</sup> were obtained from CrysTec GmbH, Germany. The substrates were sonicated in acetone and ethanol for 15 min each prior to an annealing with a dwell time of about 8 h at 1050 °C ((0001)-Zn) or 1180 °C ((000-1)-O) in an electric furnace under an O<sub>2</sub> flow of 0.1 L min<sup>-1</sup>. Kobayashi et al. showed that the ZnO surface can be significantly improved to an atomically flat, terraced structure when the substrates are placed in a small box made out of ceramic ZnO during annealing.<sup>[67]</sup> This technique was adopted and simplified by placing the ZnO wafers in a quartz glass combustion vessel covered by a planar ZnO sputtering target (99.99% purity). The sputtering target was slightly etched with acetic acid prior to every

use. After allowing the furnace to cool down to room temperature, the substrates were taken out and subsequently again sonicated in ethanol for 15 min and blown dry in a N<sub>2</sub> stream. Afterwards the substrates were immediately immersed to the molecule solution. Recycling of the substrates for multiple usages has been performed by a three step hand-polishing procedure with 1) 1 μm diamond suspension, 2) 0.25 μm diamond suspension, and 3) pure ethanol followed by the procedure described above, yielding terraced surface structures comparable to industrially polished substrates.

**Preparation of Phosphonic Acids and of Self-Assembled Monolayers:** Benzylophosphonic acid (BPA, 97%), 4-bromobenzylphosphonic acid (BrBPA, 97%), 4-fluorobenzylphosphonic acid (FBPA, 99%), pentafluorobenzylphosphonic acid (5FBPA, 97%), and 4-aminobenzylphosphonic acid (ABPA, >95%) have been obtained from Sigma Aldrich and were used without further purification. (Pyrimidin-2-yl) methylphosphonic acid (PyPA) and 4-trifluoromethylbenzylphosphonic acid (3FMBPA) have been synthesized via alkylation of triethyl phosphite with the corresponding benzylic halide followed by acidic hydrolysis of the formed diethyl benzylic phosphonate. PyPA: 2-Chloromethylpyrimidine<sup>[68]</sup> (1.30 g, 10.11 mmol) and triethyl phosphite (3.46 g, 20.22 mmol) were refluxed for 18 h. The excess triethyl phosphite was removed in vacuo and the residue subjected to column chromatography (CH<sub>2</sub>Cl<sub>2</sub> : MeOH = 100 : 4) to yield 1.52 g (65%) of the intermediate diethyl (pyrimidin-2-yl)methyl phosphonate. <sup>1</sup>H-NMR (300 MHz, CD<sub>2</sub>Cl<sub>2</sub>): δ (ppm) = 1.30 (t, J = 9 Hz, 3H), 3.55 (d, J = 21 Hz, 2H), 4.12 (m, 4H), 7.23 (m, 1H), 8.71 (d, J = 3 Hz, 2H). To the intermediate diethyl (pyrimidin-2-yl) methyl phosphonate (0.50 g, 2.17 mmol) in 30 mL of acetonitrile was added trimethylsilylbromide (0.86 g, 6.51 mmol) dropwise at 0 °C. The obtained solution was stirred overnight and the solvent was removed in vacuo. After 10 mL of MeOH were added, the suspension was stirred for 30 min, and the solvent removed under reduced pressure. Once again 10 mL of MeOH were added and the white solid formed was isolated by filtration. Recrystallization from MeOH/H<sub>2</sub>O afforded 0.32 g (85%) of the desired (pyrimidin-2-yl)methyl phosphonic acid. <sup>1</sup>H-NMR (300 MHz, D<sub>2</sub>O): δ (ppm) = 3.51 (d, J = 21 Hz, 2H), 7.75 (m, 1H), 8.95 (2H, J = 3 Hz, 2H). <sup>13</sup>C-NMR (75 MHz, D<sub>2</sub>O) 37.9 (J = 120 Hz), 120.4, 157.7, 161.5. 3FMBPA was prepared according to a literature procedure.<sup>[69]</sup> SAMs were prepared by immersing properly prepared ZnO wafers for a given time in a 2 mM solution of the respective BPA in dried ethanol (SeccoSolv, Merck Millipore, <0.01% H<sub>2</sub>O). In order to reduce contaminations, the preparation was performed in a N<sub>2</sub> filled glovebox and by using solely PTFE vessels and holders. After immersion, the substrates were gently purged in dried ethanol and subsequently dried with a N<sub>2</sub>-stream followed by an annealing step for 3 min at 90 °C on a hot plate.

**Kelvin Probe:** Work functions were measured in a N<sub>2</sub>-filled glovebox at room temperature with an SKM KP 4.5 (KP Technology Ltd.) with 2 mm probe diameter. Calibration of the tip work function was done against highly ordered pyrolytic graphite (HOPG), for which we assumed a work function of 4.6 eV.<sup>[44]</sup>

**AFM and SKPM:** Atomic force microscopy and scanning Kelvin probe microscopy have been performed using a NT-MDT Solver PRO with a 100 × 100 × 5 μm<sup>3</sup> hardware-linearized scanner in ambient conditions at room temperature. AFM scanning was carried out in semi-contact mode (according to tapping mode). SKPM was measured in the two-pass technique with a resolution of about 1 mV. NT-MDT NSG10 non-contact cantilevers with 10 nm PtIr coating, a typical curvature radius of the tip of 35 nm and a resonance frequency of about 240 kHz were used.

**NEXAFS:** The NEXAFS spectra were acquired in the Partial Electron Yield (PEY) mode at the HE-SGM beamline at the synchrotron radiation facility BESSY II in Berlin (Germany). The endstation was equipped with home-made NEXAFS detector and a five-axis manipulator with a liquid Helium cooling system in the analysis chamber.<sup>[70]</sup> The base pressures in the analysis chamber and preparation chamber were better than 5 × 10<sup>-10</sup> Torr and 2 × 10<sup>-9</sup> Torr, respectively. The degree of polarization of the incident synchrotron light at HE-SGM beamline was amounted to 0.91. To control a possible degradation of BPA under synchrotron radiation, the NEXAFS spectra were measured a few times for every incidence

angle and compared to each other. Fortunately, no changes were found in the experimental spectra, indicating a very low degree of radiation degradation of the BPA SAMs during the NEXAFS measurements.

**XRR:** In X-ray reflectivity (XRR) the intensity of the specularly reflected X-ray beam *R* as a function of the angle of incidence *θ* is measured. The vector *q<sub>z</sub>* is the momentum transfer in the direction of the surface normal *z* and can be calculated as a function of the angle of incidence *θ* of the X-ray beam using  $q_z = 4\pi \lambda^{-1} \sin\theta$ . The XRR curves of BPA, 5FBPA and 3FMBPA were acquired on an X-ray diffractometer with a rotating Cu-Kα anode source. The measurements were performed in a high vacuum (HV) chamber at a pressure of 10<sup>-6</sup> to 10<sup>-7</sup> mbar to avoid beam damage by ozone. A substrate temperature of 100 °C was used to minimize water adsorption on the sample.

The presented data contains a geometrical footprint correction, to compensate for the flux not hitting the sample at small angles, and a subtracted offset scan to obtain the true reflectivity without diffuse scattering. To extract the thickness of the SAM *d* and its electron density *ρ<sub>el</sub>* the data were fitted using the software Parratt 32 version 1.6,<sup>[71]</sup> which is based on the Parratt Formalism.<sup>[72]</sup> For each fit a constant detector background of 1 × 10<sup>-7</sup> counts was assumed.

**Single Carrier Devices:** For the preparation of hole- or electron-only devices, layers of poly(3-hexylthiophene-2,5-diyl) (P3HT) or phenyl-C<sub>71</sub>-butyric-acid-methyl ester (PCBM) were prepared by spincoating from chloroform solution on top of the SAM-modified ZnO substrates, with a resulting thickness of 310 nm and 350 nm, respectively. Subsequently, Ag top electrodes with a thickness of 100 nm and an area of 2 mm<sup>2</sup> have been evaporated on top. For *J*-*V* measurements, the ZnO substrates were glued with a thin extensive layer of silver paint on top of a larger gold-covered glass substrate, which was contacted to a wire with silver paint. Contact to the top electrodes was realized with a 0.1 mm gold wire.

**DFT:** DFT calculations were performed with the B3LYP<sup>[73-75]</sup> exchange-correlation potential (as implemented in Gaussian 09, Rev. A.02)<sup>[76]</sup> and the triple-ζ, DFT-optimized, polarization-consistent pc2 basis set of Jensen.<sup>[77,78]</sup>

## Supporting Information

Supporting Information is available from the Wiley Online Library or from the author.

## Acknowledgements

The authors thank Maria Buchholz from Karlsruhe Institute of Technology and Melanie Timpel from Humboldt-Universität zu Berlin for experimental assistance and discussion. They also acknowledge several stimulating discussions with Prof. Norbert Koch from the Humboldt University Berlin. The work was supported by the German Research Foundation (DFG via SFB 951 "HIOS"). A.N. and C.W. acknowledge funding from the "Science and Technology of Nanosystems" Programme (Project No. 431103-Molecular Building Blocks/Supramolecular Networks).

Received: May 8, 2014

Revised: July 9, 2014

Published online:

- [1] T. Minami, *Semicond. Sci. Technol.* **2005**, *20*, S35.
- [2] V. Bhosle, J. T. Prater, F. Yang, D. Burk, S. R. Forrest, J. Narayan, *J. Appl. Phys.* **2007**, *102*, 023501.
- [3] J. Owen, M. S. Son, K.-H. Yoo, B. D. Ahn, S. Y. Lee, *Appl. Phys. Lett.* **2007**, *90*, 033512.
- [4] Y. H. Kim, J. S. Kim, W. M. Kim, T.-Y. Seong, J. Lee, L. Müller-Meskamp, K. Leo, *Adv. Funct. Mater.* **2013**, *23*, 3645.

- [5] C. Wöll, *Prog. Surf. Sci.* **2007**, *82*, 55.
- [6] J. C. Bernède, L. Cattin, M. Morsli, Y. Berredjem, *Sol. Energ. Mater. Sol. C.* **2008**, *92*, 1508.
- [7] K. N. Pradipta, Y. Jihoon, K. Jinwoo, C. Seungjun, J. Jaewook, L. Changhee, H. Yongtaek, *J. Phys. D: Appl. Phys.* **2009**, *42*, 035102.
- [8] M. Jørgensen, K. Norrman, F. C. Krebs, *Sol. Energ. Mater. Sol. C.* **2008**, *92*, 686.
- [9] J.-H. Park, S. J. Kang, S.-I. Na, H. H. Lee, S.-W. Kim, H. Hosono, H.-K. Kim, *Sol. Energ. Mater. Sol. C.* **2011**, *95*, 2178.
- [10] G. Heimel, L. Romaner, E. Zojer, J.-L. Brédas, *Acc. Chem. Res.* **2008**, *41*, 721.
- [11] P. J. Hotchkiss, H. Li, P. B. Paramonov, S. A. Paniagua, S. C. Jones, N. R. Armstrong, J.-L. Brédas, S. R. Marder, *Adv. Mater.* **2009**, *21*, 4496.
- [12] A. Sharma, A. Haldi, P. J. Hotchkiss, S. R. Marder, B. Kippelen, *J. Appl. Phys.* **2009**, *105*, 074511.
- [13] B. A. MacLeod, N. E. Horwitz, E. L. Ratcliff, J. L. Jenkins, N. R. Armstrong, A. J. Giordano, P. J. Hotchkiss, S. R. Marder, C. T. Campbell, D. S. Ginger, *J. Phys. Chem. Lett.* **2012**, *3*, 1202.
- [14] K. M. Knesting, P. J. Hotchkiss, B. A. MacLeod, S. R. Marder, D. S. Ginger, *Adv. Mater.* **2012**, *24*, 642.
- [15] A. Bulusu, S. A. Paniagua, B. A. MacLeod, A. K. Sigdel, J. J. Berry, D. C. Olson, S. R. Marder, S. Graham, *Langmuir* **2013**, *29*, 3935.
- [16] H.-L. Yip, S. K. Hau, N. S. Baek, A. K.-Y. Jen, *Appl. Phys. Lett.* **2008**, *92*, 193313.
- [17] N. H. Moreira, A. L. da Rosa, T. Frauenheim, *Appl. Phys. Lett.* **2009**, *94*, 193109.
- [18] X. Tian, J. Xu, W. Xie, *J. Phys. Chem. C* **2010**, *114*, 3973.
- [19] K. Ozawa, T. Hasegawa, K. Edamoto, K. Takahashi, M. Kamada, *J. Phys. Chem. B* **2002**, *106*, 9380.
- [20] L. Thomsen, B. Watts, P. C. Dastoor, *Surf. Interface Anal.* **2006**, *38*, 1139.
- [21] C. G. Allen, D. J. Baker, J. M. Albin, H. E. Oertli, D. T. Gillaspie, D. C. Olson, T. E. Furtak, R. T. Collins, *Langmuir* **2008**, *24*, 13393.
- [22] C. Nogue, P. Lang, *Langmuir* **2007**, *23*, 8385.
- [23] P. W. Sadik, S. J. Pearton, D. P. Norton, E. Lambers, F. Ren, *J. Appl. Phys.* **2007**, *101*, 104514.
- [24] C. L. Rhodes, S. Lappi, D. Fischer, S. Sambasivan, J. Genzer, S. Franzen, *Langmuir* **2007**, *24*, 433.
- [25] C. L. Perkins, *J. Phys. Chem. C* **2009**, *113*, 18276.
- [26] J. Chen, R. E. Ruther, Y. Tan, L. M. Bishop, R. J. Hamers, *Langmuir* **2012**, *28*, 10437.
- [27] P. J. Hotchkiss, M. Malicki, A. J. Giordano, N. R. Armstrong, S. R. Marder, *J. Mater. Chem.* **2011**, *21*, 3107.
- [28] B. Zhang, T. Kong, W. Xu, R. Su, Y. Gao, G. Cheng, *Langmuir* **2010**, *26*, 4514.
- [29] C. Wood, H. Li, P. Winget, J.-L. Brédas, *J. Phys. Chem. C* **2012**, *116*, 19125.
- [30] T. M. Brenner, G. Chen, E. P. Meinig, D. J. Baker, D. C. Olson, R. T. Collins, T. E. Furtak, *J. Mater. Chem. C* **2013**, *1*, 5935.
- [31] N. Kedem, S. Blumstengel, F. Henneberger, H. Cohen, G. Hodes, D. Cahen, *Phys. Chem. Chem. Phys.* **2014**, *16*, 8310.
- [32] O. Taratula, E. Galoppini, D. Wang, D. Chu, Z. Zhang, H. Chen, G. Saraf, Y. Lu, *J. Phys. Chem. B* **2006**, *110*, 6506.
- [33] M. Gliboff, L. Sang, K. M. Knesting, M. C. Schallnat, A. Mudalige, E. L. Ratcliff, H. Li, A. K. Sigdel, A. J. Giordano, J. J. Berry, D. Nordlund, G. T. Seidler, J.-L. Brédas, S. R. Marder, J. E. Pemberton, D. S. Ginger, *Langmuir* **2013**, *29*, 2166.
- [34] D. A. Egger, F. Rissner, G. M. Rangger, O. T. Hofmann, L. Wittwer, G. Heimel, E. Zojer, *Phys. Chem. Chem. Phys.* **2010**, *12*.
- [35] D. A. Egger, F. Rissner, E. Zojer, G. Heimel, *Adv. Mater.* **2012**, *24*, 4291.
- [36] H. Li, P. Paramonov, J.-L. Brédas, *J. Mater. Chem.* **2010**, *20*, 2630.
- [37] J. R. Macdonald, C. A. Barlow, *J. Chem. Phys.* **1963**, *39*, 412.
- [38] B. L. Maschhoff, J. P. Cowin, *J. Chem. Phys.* **1994**, *101*, 8138.
- [39] G. Heimel, L. Romaner, E. Zojer, J.-L. Brédas, *Nano Lett.* **2007**, *7*, 932.
- [40] L. Romaner, G. Heimel, C. Ambrosch-Draxl, E. Zojer, *Adv. Funct. Mater.* **2008**, *18*, 3999.
- [41] A. Natan, N. Kuritz, L. Kronik, *Adv. Funct. Mater.* **2010**, *20*, 2077.
- [42] A. Natan, L. Kronik, H. Haick, R. T. Tung, *Adv. Mater.* **2007**, *19*.
- [43] M. Valtiner, X. Torrelles, A. Pareek, S. Borodin, H. Gies, G. Grundmeier, *J. Phys. Chem. C* **2010**, *114*, 15440.
- [44] M. M. Beerbom, B. Lägél, A. J. Cascio, B. V. Doran, R. Schlaf, *J. Electron. Spectrosc.* **2006**, *152*, 12.
- [45] F. Traeger, M. Kauer, C. Wöll, D. Rogalla, H. W. Becker, *Phys. Rev. B* **2011**, *84*, 075462.
- [46] J. Stöhr, *NEXAFS Spectroscopy*, Springer-Verlag, Berlin, Germany **1992**.
- [47] I. M. Tidswell, B. M. Ocko, P. S. Pershan, S. R. Wasserman, G. M. Whitesides, J. D. Axe, *Phys. Rev. B* **1990**, *41*, 1111.
- [48] H. Li, L. K. Schirra, J. Shim, H. Cheun, B. Kippelen, O. L. A. Monti, J.-L. Brédas, *Chem. Mater.* **2012**, *24*, 3044.
- [49] H. Li, E. L. Ratcliff, A. K. Sigdel, A. J. Giordano, S. R. Marder, J. J. Berry, J.-L. Brédas, *Adv. Funct. Mater.* **2014**, *24*.
- [50] S. Braun, W. R. Salaneck, M. Fahlman, *Adv. Mater.* **2009**, *21*, 1450.
- [51] J. Hwang, A. Wan, A. Kahn, *Mater. Sci. Eng. R* **2009**, *64*, 1.
- [52] J. C. Blakesley, N. C. Greenham, *J. Appl. Phys.* **2009**, *106*, 034507.
- [53] I. Lange, J. C. Blakesley, J. Frisch, A. Vollmer, N. Koch, D. Neher, *Phys. Rev. Lett.* **2011**, *106*, 216402.
- [54] M. T. Greiner, M. G. Helander, W.-M. Tang, Z.-B. Wang, J. Qiu, Z.-H. Lu, *Nat. Mater.* **2012**, *11*, 76.
- [55] L. Ley, Y. Smets, C. I. Pakes, J. Ristein, *Adv. Funct. Mater.* **2013**, *23*, 794.
- [56] F. J. Zhang, A. Vollmer, J. Zhang, Z. Xu, J. P. Rabe, N. Koch, *Org. Electron.* **2007**, *8*, 606.
- [57] Z.-L. Guan, J. Bok Kim, Y.-L. Loo, A. Kahn, *J. Appl. Phys.* **2011**, *110*, 043719.
- [58] J. E. Lyon, A. J. Cascio, M. M. Beerbom, R. Schlaf, Y. Zhu, S. A. Jenekhe, *Appl. Phys. Lett.* **2006**, *88*, 222109.
- [59] M. C. Scharber, D. Mühlbacher, M. Koppe, P. Denk, C. Waldauf, A. J. Heeger, C. J. Brabec, *Adv. Mater.* **2006**, *18*, 789.
- [60] I. Lange, J. Kniepert, P. Pingel, I. Dumsch, S. Allard, S. Janietz, U. Scherf, D. Neher, *J. Phys. Chem. Lett.* **2013**, *4*, 3865.
- [61] Z. Xu, L.-M. Chen, M.-H. Chen, G. Li, Y. Yang, *Appl. Phys. Lett.* **2009**, *95*, 013301.
- [62] Z. B. Wang, M. G. Helander, M. T. Greiner, J. Qiu, Z. H. Lu, *Phys. Rev. B* **2009**, *80*, 235325.
- [63] H. T. Nicolai, M. M. Mandoc, P. W. M. Blom, *Phys. Rev. B* **2011**, *83*, 195204.
- [64] Y. Zhang, P. W. M. Blom, *Appl. Phys. Lett.* **2011**, *98*, 143504.
- [65] P. de Bruyn, A. H. P. van Rest, G. A. H. Wetzelaer, D. M. de Leeuw, P. W. M. Blom, *Phys. Rev. Lett.* **2013**, *111*, 186801.
- [66] G. A. H. Wetzelaer, A. Najafi, R. J. P. Kist, M. Kuik, P. W. M. Blom, *Appl. Phys. Lett.* **2013**, *102*, 053301.
- [67] K. Atsushi, O. Jitsuo, F. Hiroshi, *Jpn. J. Appl. Phys.* **2006**, *45*, 5724.
- [68] R. Thomas, J. Stetter, L. Eue, R. R. Schmidt, US patent 4328029, 1982.
- [69] C. Schwender, K. Demarest, D. Wustrow, US patent 5300687, 1994.
- [70] A. Nefedov, C. Wöll, in *Surface Science Techniques, Springer Series in Surface Science* (Eds: G. Bracco, B. Holst), Springer, Berlin, Heidelberg, Germany **2013**, p. 277–301.
- [71] C. Braun, *Parratt32*, Hahn-Meitner-Institut, Berlin, Germany **2002**.
- [72] L. G. Parratt, *Phys. Rev.* **1954**, *95*, 359.
- [73] A. D. Becke, *Phys. Rev. A* **1988**, *38*, 3098.
- [74] C. Lee, W. Yang, R. G. Parr, *Phys. Rev. B* **1988**, *37*, 785.

- [75] A. D. Becke, *J. Chem. Phys.* **1993**, *98*, 5648.
- [76] M. J. Frisch, G. W. Trucks, H. B. Schlegel, G. E. Scuseria, M. A. Robb, J. R. Cheeseman, G. Scalmani, V. Barone, B. Mennucci, G. A. Petersson, H. Nakatsuji, M. Caricato, X. Li, H. P. Hratchian, A. F. Izmaylov, J. Bloino, G. Zheng, J. L. Sonnenberg, M. Hada, M. Ehara, K. Toyota, R. Fukuda, J. Hasegawa, M. Ishida, T. Nakajima, Y. Honda, O. Kitao, H. Nakai, T. Vreven, J. A. Montgomery, Jr., J. E. Peralta, F. Ogliaro, M. Bearpark, J. J. Heyd, E. Brothers, K. N. Kudin, V. N. Staroverov, R. Kobayashi, J. Normand, K. Raghavachari, A. Rendell, J. C. Burant, S. S. Iyengar, J. Tomasi, M. Cossi, N. Rega, J. M. Millam, M. Klene, J. E. Knox, J. B. Cross, V. Bakken, C. Adamo, J. Jaramillo, R. Gomperts, R. E. Stratmann, O. Yazyev, A. J. Austin, R. Cammi, C. Pomelli, J. W. Ochterski, R. L. Martin, K. Morokuma, V. G. Zakrzewski, G. A. Voth, P. Salvador, J. J. Dannenberg, S. Dapprich, A. D. Daniels, Ö. Farkas, J. B. Foresman, J. V. Ortiz, J. Cioslowski, D. J. Fox, Gaussian 09, Revision A.02, Gaussian Inc., Wallingford CT **2009**.
- [77] F. Jensen, *J. Chem. Phys.* **2001**, *115*, 9113.
- [78] F. Jensen, *J. Chem. Phys.* **2002**, *116*, 3502.
- [79] M. Timpel, M. V. Nardi, S. Krause, G. Ligorio, C. Christodoulou, L. Pasquali, A. Giglia, J. Frisch, B. Wegner, P. Moras, N. Koch, *Chem. Mater.* **2014**, *10.1021/cm502171m*.